

This item is likely protected under Title 17 of the U.S. Copyright Law. Unless on a Creative Commons license, for uses protected by Copyright Law, contact the copyright holder or the author.

Access to this work was provided by the University of Maryland, Baltimore County (UMBC) ScholarWorks@UMBC digital repository on the Maryland Shared Open Access (MD-SOAR) platform.

**Please provide feedback**

Please support the ScholarWorks@UMBC repository by emailing [scholarworks-group@umbc.edu](mailto:scholarworks-group@umbc.edu) and telling us what having access to this work means to you and why it's important to you. Thank you.

# Electromagnetic fields generated by a three dimensional global ocean circulation

Robert H. Tyler<sup>1</sup> and Lawrence A. Mysak

Department of Atmospheric and Oceanic Sciences and Centre for Climate and Global Change Research, McGill University, Montréal, Québec, Canada

Josef M. Oberhuber

Deutsches Klimarechenzentrum GmbH, Hamburg, Germany

**Abstract.** A simplified form of the motional induction equation is used to calculate the dominant three-dimensional (3-D) electromagnetic (EM) fields generated by a specified steady 3-D global ocean circulation. The EM calculations require, at most, vertical integrations and do not require running a global 3-D model. Two cases for ocean bottom conductivity are considered: an electrically insulating ocean bottom and a high-conductance sediment layer. The approximations are discussed, and the solutions are plotted for various depth levels. Many aspects of the dominant ocean-generated EM fields (particularly the electric currents near the sea surface and the magnetic fields) are shown to be insensitive to ocean bottom conductivity. Other aspects (particularly the horizontal electric field in shallow water) are very sensitive. We perform a global integration to estimate the role of the “nonlocal” electric currents. We find that the importance in including these nonlocal currents when making EM field estimates is the same or less than that for including a model for the bottom conductance. Hence the simple EM estimates from one-dimensional integrations are not improved in globally integrated models until these models include a realistic model for bottom conductivity.

## 1. Introduction

The ocean is a conducting fluid. As it flows through the Earth's main magnetic field, it induces electric currents, spatial charge densities, and associated magnetic and electric fields. In recent papers [Tyler and Mysak, 1995a, b], we presented extensions of the theory of oceanic motionally induced electromagnetic fields [e.g., Sanford, 1971; Chave and Luther, 1990]. Here we focus on calculating and plotting the dominant three-dimensional (3-D) electromagnetic (EM) fields induced by a prescribed steady 3-D global ocean circulation.

A better understanding of the ocean-generated EM fields is of interest for several reasons. First, since the early pioneering work of Sanford [1982], Larsen and Sanford [1985], and Filloux [1987], ocean EM fields have been of increasing interest to oceanographers in studies of ocean flow. Ocean EM fields are also relevant to geophysicists studying geological structures beneath the ocean [see Chave *et al.*, 1988]. A better understand-

ing of the sensitivity of the ocean-generated EM fields to ocean bottom conductance, for example, has direct bearing on these efforts. Secondly if it can be established that the oceans generate magnetic signals which are recorded at inland and satellite magnetic observatories, then it may be possible to use magnetic field observations as a remote-sensing tool for oceanographic applications. The difficulties and potential benefits of this are discussed by Tyler [1995]. Finally, it would be of interest to geophysicists studying the global Earth's magnetic field to know which contributions of the Earth's magnetic field and its variability are oceanic in origin. The results we will present address the dominant ocean-induced EM fields within the oceans and have the most direct bearing on the first of the items above. In particular, we wish to help understand to what extent local ocean flow can be associated with locally measured EM fields (in principle, EM observations at a point could depend on global ocean flow) when the conductivity distribution below the ocean is unknown.

“Motional electromagnetic induction” is distinguished from “electromagnetic induction” appearing in other subjects (such as magnetotellurics) by the focus of attention on the EM fields induced by motion of the conductor through an ambient magnetic field. Another distinguishing feature of the motional induction case is that kinetic energy (of the ocean flow) is converted

<sup>1</sup>Now at Applied Physics Laboratory, University of Washington, Seattle.

to EM energy. This point should be made clear since the ocean is important both as an “inductor” and as a “motional inductor.” For example, simply because the ocean is relatively conductive, time-varying magnetic fields originating in the ionosphere induce electric currents in the ocean. In this paper we are not concerned with this effect, only with that of motional induction due to ocean velocities. For the rest of this paper, expressions such as “ocean-induced EM fields” should be understood to mean the more restrictive case of just motional induction. We assume here a frame of reference moving with the solid Earth. The conductor velocities involved are then the customary ocean current velocities. Use of the induction equation in a rotating frame of reference requires justification, which is given by *Tyler and Mysak* [1995a].

The theoretical foundations for 3-D motional induction in the ocean were laid out by *Sanford* [1971]. During the past 2 decades, other works have extended the theory [e.g., *Larsen*, 1973; *Chave*, 1983; *Chave and Luther*, 1990; *Stephenson and Bryan*, 1992; *Tyler*, 1995; *Tyler and Mysak*, 1995b], and a recent review is given by *Larsen* [1992].

Turning now toward the descriptive and applied aspects, several papers [*Bindoff et al.*, 1986; *Lilley et al.*, 1986, 1993; *Larsen and Sanford*, 1985; *Sanford*, 1982] discuss limited observations of the EM fields in the ocean. *Stephenson and Bryan* [1992] performed a two-dimensional (2-D) numerical study of the EM fields induced by a coarse-resolution global ocean circulation. Recently, *Flosadóttir et al.* [1994] have done a numerical calculation of the EM fields produced by a realistic 3-D flow in the North Atlantic which included realistic sediments. In their study they claim to find little evidence for nonlocalized electric current loops but rather find good support for the “Sanford approximation.” Under this approximation, calculations of the EM fields require at most vertical integrations over the ocean and underlying conductivity layers. This approximation is further justified in the next section, and in section 5 we estimate the potential errors in our results arising from not resolving these nonlocal currents. We emphasize that this approximation only applies when calculating the dominant EM fields within the ocean. The ocean-induced large-scale EM fields will also reach outside of the ocean. In these regions, however, the approximation above does not apply.

The purpose of this paper is twofold. First, we wish to calculate and plot the patterns of the global EM fields induced by a steady global ocean circulation. This should give a general overview of the magnitudes and locations of the dominant global ocean-generated EM fields. Second, since the ocean EM fields depend on the distribution of electrical conductivity below the ocean and this distribution is not well known, we wish to estimate the maximum uncertainties in EM field estimates due to the uncertainties in the ocean bottom conductance.

In the next section we discuss the equations that govern the EM fields generated by ocean currents. In section 3 we describe the ocean circulation model that was used to generate the ocean flow and conductivity fields; we describe the two limiting case models that will be assumed for the ocean bottom conductance, and then we show the calculated EM fields and estimate the fractional uncertainties in these fields. In section 4 we discuss the effects of nonlocal electric currents. Finally, in section 5, we discuss and summarize the results.

## 2. Governing Equations

The motional induction equation applicable to the ocean is

$$\partial_t \mathbf{B} = \nabla \times (\mathbf{u} \times \mathbf{B} - K \nabla \times \mathbf{B}) \quad (1)$$

[*Tyler and Mysak*, 1995a] where  $\mathbf{B}$  is the magnetic field (teslas),  $\mathbf{u}$  is the ocean velocity relative to the Earth (meters per second), and  $K = (\mu_o \sigma)^{-1}$  is the magnetic diffusivity (square meters per second) with  $\sigma$  the electrical conductivity (siemens per meter) and  $\mu_o$  the vacuum magnetic permeability (henries per meter).

The first term on the right-hand side of (1) can be viewed as a source term due to a prescribed ocean velocity field, while the second term describes magnetic dissipation or losses due to Ohmic heating. The losses take place only in the regions where there is an electrical current  $\mathbf{J}$ . This can be seen from Ampere's law

$$\nabla \times \mathbf{B} = \mu_o \mathbf{J}. \quad (2)$$

Thus the loss term in (1) will vanish where  $\mathbf{J} = 0$ .

A useful decomposition is  $\mathbf{B} = \mathbf{F} + \mathbf{b}$ , where  $\mathbf{F}$  is the Earth's main magnetic field due to electric currents in the Earth's core and  $\mathbf{b}$  is the magnetic field induced by electric currents generated in the ocean's velocity. We will not consider domains including the Earth's core so the source currents for  $\mathbf{F}$  are zero in the region where (1) is to be solved. Therefore we have  $\nabla \times \mathbf{F} = 0$ . Also, we will only consider the steady state case, so (1) for our case becomes

$$\nabla \times (K \nabla \times \mathbf{b}) = \nabla \times (\mathbf{u} \times \mathbf{B}). \quad (3)$$

To proceed further, let us consider a Cartesian coordinate frame similar to that typically used in oceanography (see Figure 1) with the usual oceanographic notation of the current velocities  $\mathbf{u} = u\hat{x} + v\hat{y} + w\hat{z}$ . However, note that we shall use subscripts to describe the magnetic vector components:  $\mathbf{B} = B_x\hat{x} + B_y\hat{y} + B_z\hat{z}$ . A subscript  $H$  refers to the horizontal components of the vector.

Magnetic fields are nondivergent ( $\nabla \cdot \mathbf{B} = 0$ ), and we also take the ocean to be incompressible ( $\nabla \cdot \mathbf{u} = 0$ ). Then, (3) can be expanded as

$$\begin{aligned} \nabla \times (K \nabla \times \mathbf{b}) &= (\mathbf{B} \cdot \nabla) \mathbf{u} - (\mathbf{u} \cdot \nabla) \mathbf{B} \\ &= [(\mathbf{B} \cdot \nabla) \mathbf{u}_H - (\mathbf{u} \cdot \nabla) \mathbf{B}_H] + [\mathbf{B} \cdot \nabla w - \mathbf{u} \cdot \nabla B_z] \hat{z}. \end{aligned} \quad (4)$$

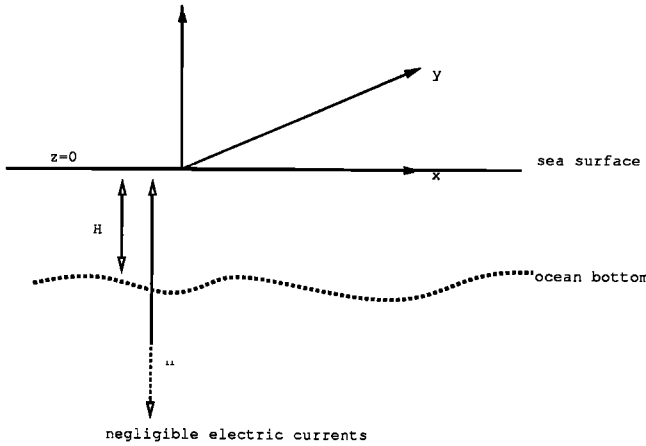


**Figure 1.** Cartesian coordinate system used in calculations.  $H$  is the ocean depth and  $h$  is a depth below which ocean-generated electric currents are negligible (typically, the depth to the bottom of the sediment layer).

Scaling arguments can be used to simplify (4). We will follow the procedure of *Tyler* [1995] and *Tyler and Mysak* [1995a, b]. For calculations in spherical coordinates, see *Stephenson and Bryan* [1992]. Briefly, we assume vertical derivatives of  $K, b_x, b_y, b_z$  are much larger than the horizontal derivatives; then we can approximate the left-hand side of (4) as

$$\nabla \times (K \nabla \times \mathbf{b}) = -\partial_z (K \partial_z \mathbf{b}_H) - (K \partial_z \partial_z b_z - \nabla K \cdot \partial_z \mathbf{b}_H) \hat{z}. \quad (5)$$

To approximate the right-hand side of (4), we start with the horizontal components. We assume  $|\mathbf{b}| \ll |\mathbf{F}|$  (this assumption can be checked later with the results). Again noting that  $|\partial_z \mathbf{u}_H| \gg |\nabla_H \cdot \mathbf{u}_H|$ , the first term is approximately  $F_z \partial_z \mathbf{u}_H$ . The second term is  $-(\mathbf{u} \cdot \nabla) \mathbf{B}_H = -(\mathbf{u}_H \cdot \nabla)(\mathbf{F}_H + \mathbf{b}_H) - w \partial_z (\mathbf{F}_H + \mathbf{b}_H)$ . Note that the spatial scale of  $\mathbf{F}$  is about an Earth radius, at least as large as the horizontal scale of  $\mathbf{u}$  and  $\mathbf{b}$ . Thus the components above involving  $\mathbf{u}_H$  are seen to be much smaller than  $F_z \partial_z \mathbf{u}_H$ , the leading part of the first term. For the large-scale steady flow we are considering where  $|w| \ll |\mathbf{u}_H|$ ,  $w \partial_z (\mathbf{F} + \mathbf{b})$  will also be much smaller than  $F_z \partial_z \mathbf{u}_H$ . Thus the dominant horizontal balance is simply

$$\partial_z (K \partial_z \mathbf{b}_H) = -F_z \partial_z \mathbf{u}_H. \quad (6)$$

Using similar scaling arguments, the vertical term on the right-hand side of (4)

$$\mathbf{B} \cdot \nabla w - \mathbf{u} \cdot \nabla B_z = -\nabla \cdot (B_z \mathbf{u}_H) + \nabla \cdot (w \mathbf{B}_H)$$

is approximately  $-\nabla \cdot (F_z \mathbf{u}_H)$ . Thus the dominant balance for the vertical magnetic components is

$$K \partial_z \partial_z b_z - \nabla K \cdot \partial_z \mathbf{b}_H = \nabla \cdot (F_z \mathbf{u}_H). \quad (7)$$

Comparing (6) and (7), we see that the “forcing” terms appearing on the right-hand side of the equa-

tions have quite different magnitudes; the ratio of the forcing in (7) to that in (6) is about the same as the ratio of the vertical and horizontal scales of the flow and is thus  $\ll 1$ . Due to the widely disparate magnitudes of the forcing terms in (6) and (7), which represent diffusive-like balances, we conclude that the dominant ocean-induced magnetic fields have vertical components which are small relative to the horizontal components. Note that these arguments apply to the fields within the ocean; outside of the ocean the horizontal components can be greatly reduced, having magnitudes similar to that of the vertical components. Hence for the steady large-scale ocean circulation we are considering, the dominant magnetic fields induced by the ocean currents can be represented as horizontally directed vectors. These dominant fields are also confined to the oceans and conductive sea bottom. This is expected due to the low conductivity of the lower atmosphere and land and the relatively small magnitude of the ocean-induced vertical magnetic field at the sea surface.

### 3. Solutions

Following *Tyler and Mysak* [1995b], we can integrate (6) once with respect to  $z$  to obtain

$$K \partial_z \mathbf{b}_H = -F_z (\mathbf{u}_H - \bar{\mathbf{u}}_H^*) + \frac{\Delta \mathbf{b}_H}{\int_{-h}^0 K^{-1} dz}, \quad (8)$$

and again to obtain

$$\mathbf{b}_H = \mathbf{b}_H(z=0) + F_z \left( s \int_{-h}^0 \frac{\mathbf{u}_H}{K} dz + \int_z^0 \frac{\bar{\mathbf{u}}_H^*}{K} dz' \right) + s \Delta \mathbf{b}_H \quad (9)$$

where

$$\bar{\mathbf{u}}_H^* = \frac{\int_{-h}^0 \sigma \mathbf{u}_H dz}{\int_{-h}^0 \sigma dz} \quad (10)$$

is a depth-integrated conductivity-weighted velocity similar to that introduced by *Sanford* [1971],  $h$  is a depth below which ocean-induced EM effects are unimportant,  $\Delta \mathbf{b}_H = \mathbf{b}_H(z=0) - \mathbf{b}_H(z=-h)$ , and

$$s = -\frac{\int_z^0 \sigma dz}{\int_{-h}^0 \sigma dz} \quad (11)$$

is a dimensionless conductivity-weighted vertical coordinate ranging from -1 and 0. Consistent with our earlier assumptions,  $\mathbf{b}_H(z > 0) \approx 0$ , and since  $\mathbf{b}_H$  is continuous, we can take  $\mathbf{b}_H(z=0) \approx 0$  in (9).

We will assume that the electric currents closing in horizontal planes can be neglected relative to the electric currents closing in a plane containing the vertical. In this case,  $\Delta \mathbf{b}_H \approx 0$  [*Tyler and Mysak*, 1995b]. In other terminology [*Sanford*, 1971], this approximation amounts to neglecting the nonlocal electric currents relative to the “local” ones. The errors involved in making this assumption are discussed in section 5.

We obtained (8) and (9) from the terms in the horizontal part of the induction equation. Another approach could have been to approximate Ampere's law  $\nabla \times \mathbf{b} = \mu_o \mathbf{J}$  as

$$-\partial_z \mathbf{b}_H \times \hat{z} \approx \mu_o \mathbf{J}_H = K^{-1} [\mathbf{u}_H \times (F_z \hat{z}) + \mathbf{E}_H] \quad (12)$$

where the last equality is obtained using Ohm's law ( $\mathbf{J} = \sigma(\mathbf{u} \times \mathbf{B} + \mathbf{E})$ ) and  $K = (\mu_o \sigma)^{-1}$ . The assumption that  $\mathbf{J}_H$  circulates predominantly in planes containing the vertical (which led to  $\Delta \mathbf{b}_H \approx 0$ ) requires that the depth integral of  $\mathbf{J}_H$  in (12) be zero, leading to

$$\bar{\mathbf{E}}_H = -\frac{\int_{-h}^0 \sigma \mathbf{u}_H \times (F_z \hat{z}) dz}{\int_{-h}^0 \sigma dz} = -F_z \bar{\mathbf{u}}_H^* \times \hat{z}, \quad (13)$$

the average of  $\mathbf{E}_H$  over the depth  $h$ . (Above, the variation of  $F_z$  with depth is neglected). Theory and observations indicate that the horizontal electric field is approximately depth-independent over the ocean depth, so  $\mathbf{E}_H \approx \bar{\mathbf{E}}_H$ . Thus, using this in (13) and substituting in (12), we obtain

$$\mathbf{J}_H = \sigma F_z (\mathbf{u}_H - \bar{\mathbf{u}}_H^*) \times \hat{z}. \quad (14)$$

Finally, (9) with  $\mathbf{b}_H(z=0)$  and  $\Delta \mathbf{b}_H$  neglected takes the form

$$\begin{aligned} \mathbf{b}_H &= F_z \left( s \int_{-h}^0 \frac{\mathbf{u}_H}{K} dz + \int_z^0 \frac{\mathbf{u}_H}{K} dz' \right) \\ &= \mu_o F_z \int_z^0 \sigma (\mathbf{u}_H - \bar{\mathbf{u}}_H^*) dz'. \end{aligned} \quad (15)$$

In the above, the vertical components of  $\mathbf{b}$  and  $\mathbf{J}$  are negligible compared to the horizontal components, so the dominant fields  $\mathbf{b}$  and  $\mathbf{J}$  in the ocean are given adequately by the horizontal components. This is not so for the electric field which has a vertical component which, to the order of approximation we have been considering, is found from Ohm's law to be

$$E_z = -\mathbf{u}_H \times \mathbf{F}_H \hat{z} = (vF_x - uF_y). \quad (16)$$

Next we will use (13)–(16) to estimate the electromagnetic fields generated by an ocean circulation as prescribed from a global ocean circulation model [Oberhuber, 1993a, b]. We note that (13) to (16) do not require a global integration but simply a local integration down from the sea surface provided the velocity and conductivity fields are known. The ocean velocities are given from model output; the conductivity is calculated according to methods described by *Apel* [1987] using model output for temperature and salinity. The conductance distribution below the ocean is, however, unknown and difficult to estimate with accuracy. We address this by considering limiting cases for the ocean bottom conductances which allow us to provide bounds for our calculations of the electromagnetic quantities.

## 4. The Dominant Electromagnetic Fields Generated by Steady Ocean Circulation

### 4.1. Description of the Ocean Circulation Model

The data (ocean velocities and conductivity) used for this study have been extracted from a global version of the ocean circulation model OPYC (stemming from the words "Ocean" and "isoPYCnal coordinates") developed by *Oberhuber* [1993a, b]. The model consists of five submodels that are coupled to each other. The five submodels describe the interior ocean, the surface mixed layer, the sea ice, an atmospheric boundary layer, and tides.

The model for the interior ocean is based on primitive equations for the momentum and contents of mass, heat, and salt in isopycnal layers. These quantities as well as the Lagrangian vertical coordinates and the sea level are prognostic variables. Horizontal mixing for momentum is a function of the local Rossby deformation radius in order to account for horizontal friction layers, while horizontal diffusion for tracers such as temperature and salinity involves some dependence on flow deformation. Vertical mixing follows the concept of entrainment/detrainment for which budgets of turbulent kinetic and mean potential energy are solved. Convection is included in a standard fashion. The model for the interior ocean is coupled to a surface mixed layer model as the concept of isopycnal coordinates breaks down near the surface when strong turbulence is present. At the surface, the ocean is forced with heat fluxes, wind stresses, and freshwater fluxes that also change the sea level, while at the bottom a well-resolved topography provides the lower boundary.

The mixed layer model computes entrainment rates out of an isopycnal layer or a detrainment rate into an isopycnal layer according to a budget equation for turbulent kinetic and mean potential energy. Wind stirring, surface buoyancy flux due to heat and freshwater fluxes, subsurface stability, and flow shear enter the diagnostic calculation. The mixed layer is part of the complete layer model, thus equations for the momentum, mass, temperature, and salinity are solved in the same manner as for the interior ocean.

The sea ice model contains both dynamics and thermodynamics and consists of equations for the horizontal ice velocity, ice and snow thickness, and ice concentration. A viscous-plastic rheology is chosen to parameterize the stress tensor in the dynamics equation, and the governing equations for the thickness of ice and snow and the concentration of ice are based on continuity equations. Further parameterizations relate heat fluxes to changes in ice and snow thickness as well as lead size or describe the conversion from snow to ice due to snow aging and snow suppression. The thermodynamic part of the sea ice model consists of a prognostic com-

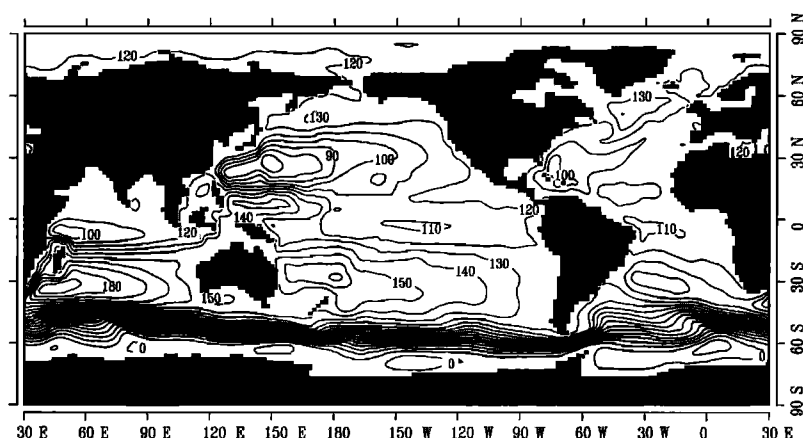


**Figure 2.** Horizontal barotropic transport stream function as simulated by OPYC in T63/L15 resolution. Units are  $10^9 \text{ kg s}^{-1}$ , which is comparable to 1 sverdrup ( $=10^6 \text{ m}^3 \text{ s}^{-1}$ ).

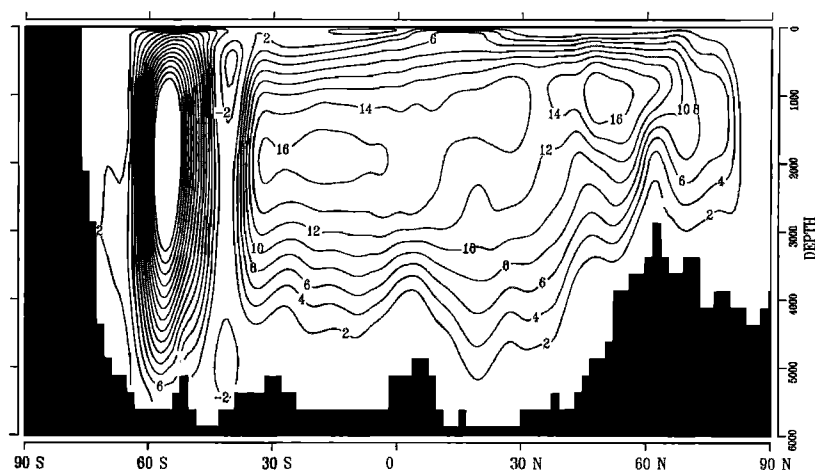
putation of the temperature profile, which results from an assumed heat capacity. Heat fluxes due to the conductivity of ice and snow and atmospheric heat fluxes control the ice and snow cover. Further details are given in Oberhuber [1993b].

Atmosphere to ocean fluxes of heat, fresh water, and as a result, buoyancy are computed from a model for the atmospheric boundary layer that is forced with atmospheric data for air temperature, humidity, cloudiness, wind speed, and rainfall. These fluxes of heat are the sum of the following: solar radiation, which is computed from orbital parameters, the solar constant, and corrections for humidity and cloudiness; outgoing long-wave radiation, which is dependent on both humidity and cloudiness; and turbulent fluxes of sensible and latent heat, which follow the bulk concept. The freshwater flux is computed from rainfall data and evaporation. Both the heat flux and the freshwater flux provide the buoyancy flux for the mixed layer model.

Finally, a tide model based on shallow water equations is coupled to the interior-ocean model via bottom stress and residual currents. The model is forced with gravitational anomalies of the major 11 tidal modes. The tide model is not essential for this study but was switched on for other ocean-only experiments.

The ocean and the sea ice models are formulated on an Arakawa B grid with no-slip horizontal boundary conditions, while the tide model is formulated on an Arakawa C grid. The ocean, ice, and tide models are fully implicit in time with alternating direction implicit (ADI) solution techniques employed.

The model version used for generating the fields required for this study has been a global model using a T63 Gaussian grid, which approximately coincides with a  $1.875^\circ$  resolution horizontally. Vertically, 15 layers have been chosen. The monthly climatological data were used, and the model was run through 100-years. A spin-up run over 1700 years on a slightly coarser T42



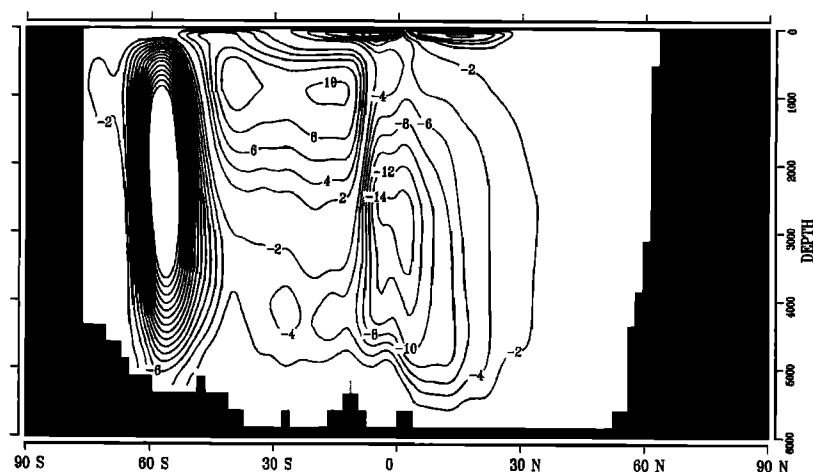


**Figure 4.** Meridional overturning transport stream function in the Pacific as simulated by OPYC in T63/L15 resolution. Units are  $10^9 \text{ kg s}^{-1}$ , which is comparable to 1 sverdrup ( $=10^6 \text{ m}^3 \text{ s}^{-1}$ ).

global resolution served as the initial condition. Therefore the ocean state was rather stationary but not fully.

To summarize in brief the model's circulation used for the study, we highlight the global ocean "conveyor belt" (discussed by *Schmitz* [1995]) with plots illustrating the barotropic stream function (Figure 2), the meridional overturning in the Atlantic (Figure 3), and the meridional overturning in the Pacific (Figure 4). In Figure 5 we show the global and basin-by-basin meridional heat transports (which can be compared with observations discussed by *Macdonald* [1993]), and the global and basin-by-basin meridional freshwater transports shown in Figure 6 can be compared with the observations reviewed by *Schmitt* [1995].

In order to conserve integral quantities, data for our later computation have been obtained by integrating over the space and time variable layers rather than performing a vertical interpolation before carrying out the various integrations. The next three figures show electrical conductivity  $\sigma$  (Figure 7), ocean conductance  $\int_H^0 \sigma dz$  (Figure 8), and the depth-integrated conductivity transport density  $\int_{-H}^0 \sigma u dz$  (Figure 9).

#### 4.2. Conductivity Below Ocean

Our EM calculations require an estimate for the total conductance  $\int_{-h}^0 \sigma dz$ , which is the sum of the ocean layer conductance  $\int_{-H}^0 \sigma dz$  (this integral is easily calcu-

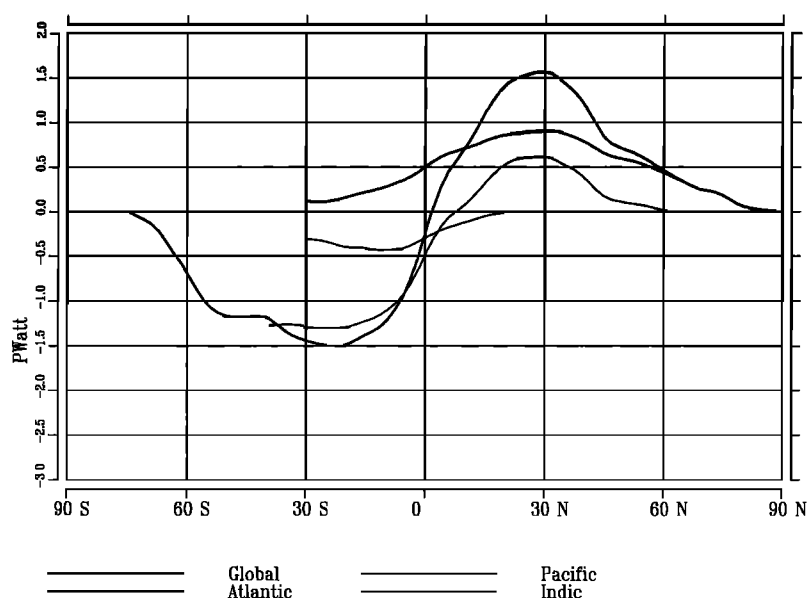


**Figure 5.** Meridional heat transport for the global ocean and for the three basins, the Atlantic, the Indic and Pacific Ocean, as simulated by OPYC in T63/L15 resolution. Units are  $10^{15} \text{ W}$  or 1 PW.

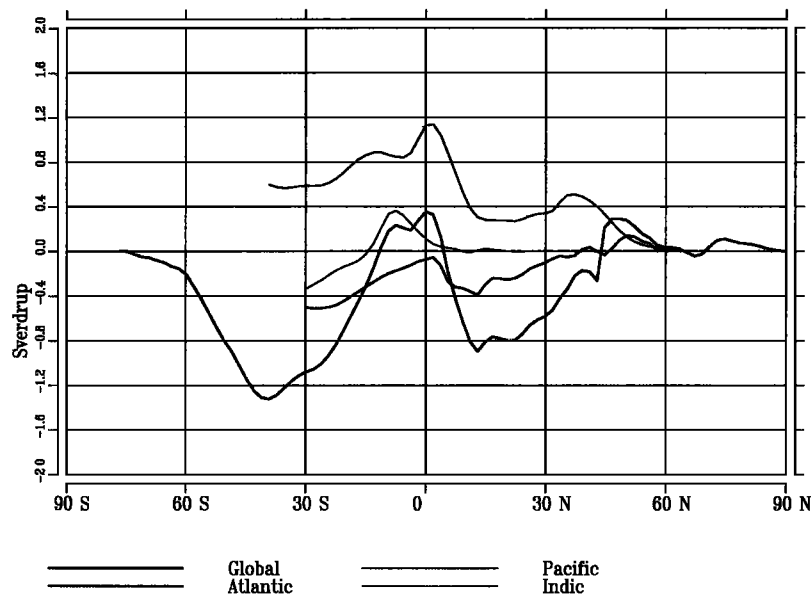


**Figure 6.** Meridional freshwater transport for the global ocean and for the three basins, the Atlantic, the Indic, and the Pacific Ocean, as simulated by OPYC in T63/L15 resolution. Units are  $10^9 \text{ kg s}^{-1}$ , which is comparable to 1 sverdrup ( $=10^6 \text{ m}^3 \text{ s}^{-1}$ ).

lated using the temperature, salinity, and ocean depth values from the ocean model and is shown in Figure 8) and the conductance  $\int_{-h}^{-H} \sigma dz$  below the ocean, what we have been calling the “ocean bottom conductance.” In principle, the ocean bottom conductance could require a vertical integration of the conductivities of all below-ocean features down to a depth of the order of the horizontal scale of the flow. In practice, however, the largest contribution to the ocean bottom conductance is simply the conductance of the sediment layer

since the region immediately below the sediments is usually regarded as an insulator for this case; *Lilley et al.* [1993] show that for the Tasman Sea, the ocean floor conductance determined from ocean EM measurements agrees with the conductance calculated for the known sediment column there. An excellent discussion of the electrical properties and relative importance of the geological features below the ocean is given by *Chave et al.* [1990].

The sediment conductance depends strongly on such

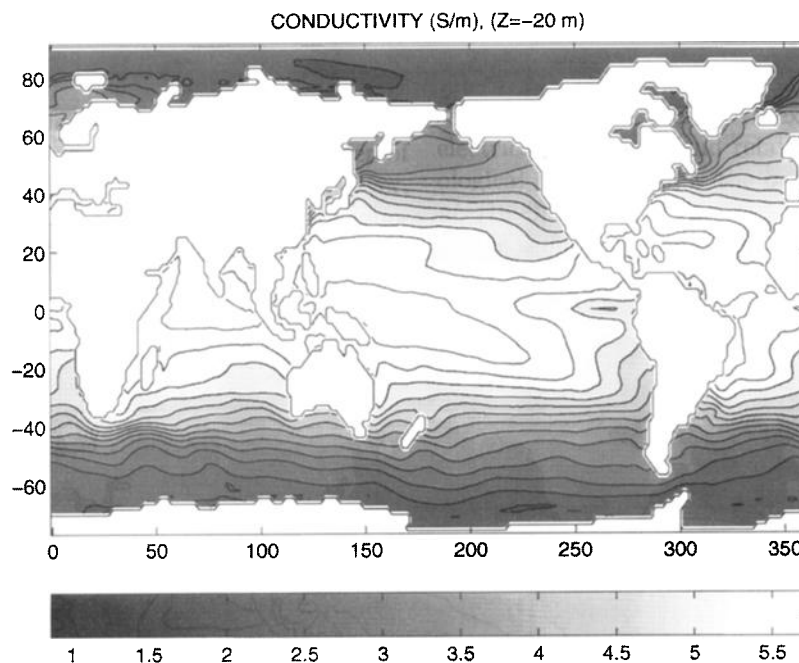


**Figure 7.** Electrical conductivity (siemens per meter) near the sea surface ( $z = -20 \text{ m}$ ). In the deeper ocean, conductivity is usually less variable with a value of about  $3\text{--}4 \text{ S m}^{-1}$ .



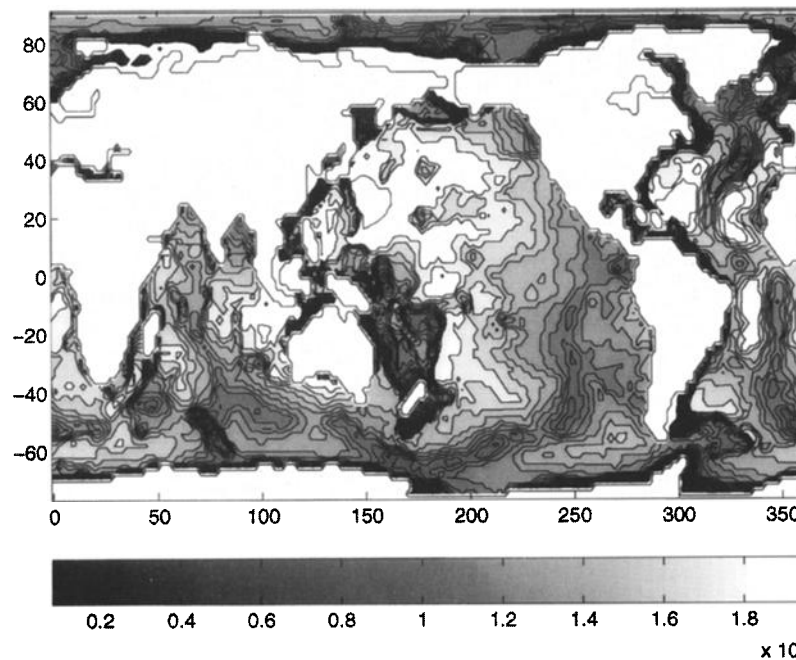


**Figure 8.** Ocean conductance, i.e. the conductivity integrated over the ocean depth (siemens).

factors as the thickness, salinity, and porosity of the sediment layer. The distribution of these quantities is very nonuniform over the ocean giving a sediment conductivity distribution that is difficult to estimate. *Flosadóttir et al.* [1997] have considered such factors to give a realistic description of the sediment conductances in the North Atlantic.

Here we need sediment conductance estimates globally. We would also like an easy interpretation for the sensitivity of the EM calculations to the sediment conductance assumptions. Hence, rather than attempting to construct a realistic model of the distribution of sediment conductance, we will consider two spatially uniform limiting cases: one in which the sediments have

zero conductance and another in which the sediments have a conductance of 3000 S, which is safely above the maximum conductance of about 2000 S shown by *Flosadóttir et al.* [1997] for the North Atlantic and a factor of 2 above maximum conductances in the Pacific and Atlantic models put forth by *Chave et al.* [1990].

To compare the relative magnitudes of the ocean and sediment conductance, the ocean will typically have a conductance  $\int_{-H}^0 \sigma dz \approx 4 \text{ (S m}^{-1}) \times H$ . So the ratio of maximum sediment conductivity over ocean conductances is unity or greater only for bottom depths  $H$  less than about 750 m. In water depths of 4000 m, the maximum sediment conductance is only about 20% that of the water column.

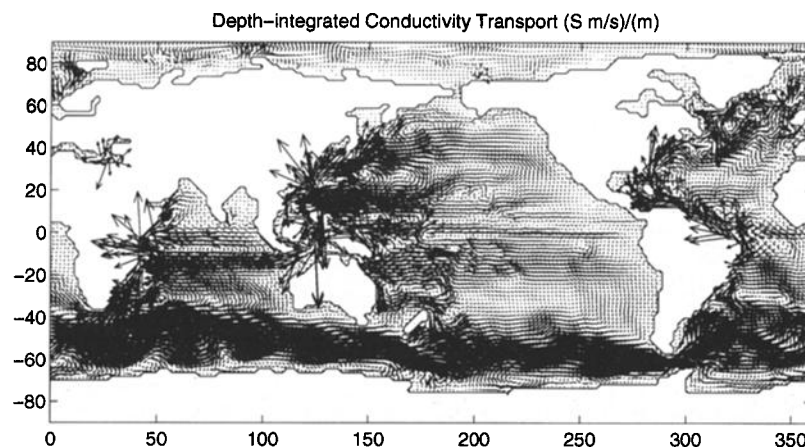


**Figure 9.** Ocean depth-integrated conductivity transport density (siemens meter per second). Scale is  $5^\circ = 10 \text{ S m s}^{-1}$ .

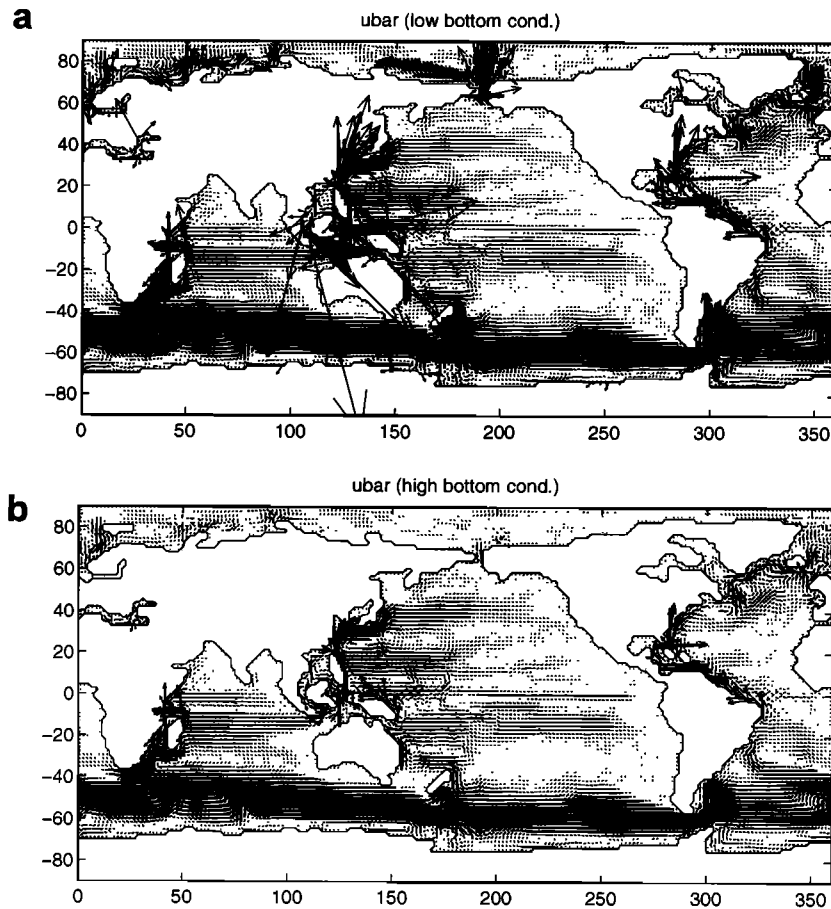


**Figure 10.** Depth-averaged  $\sigma$ -weighted velocity  $\bar{\mathbf{u}}^*$  is shown for (a) low, and (b) high, limiting cases of ocean bottom conductance. Scale is  $30^\circ = 0.1 \text{ m s}^{-1}$ . The disagreement between Figures 10a and 10b is greatest in shallow water.

#### 4.3. The Electromagnetic Fields

We will estimate the EM fields for two limiting cases of bottom conductance and plot the differences between these EM solutions sets to give an indication of the uncertainties that could be attached to EM field solutions calculated under either one of the assumptions. In this subsection we focus on describing the dominant global ocean EM fields which occur predominantly in the Antarctic Circumpolar Current and in western boundary currents. The plots here, however, give no indication of what uncertainties we should expect in regions where the ocean-generated EM fields are weak. This topic is treated in the next subsection. Also, recall that in this paper we do not treat the secondary EM fields reaching outside of the ocean.

For the purpose of organizing our plots, we note that the assumptions concerning the ocean bottom conductivity only enter through the effect on  $\bar{\mathbf{u}}_H^*$  (which is why we have written (13)–(15) in terms of  $\bar{\mathbf{u}}_H^*$ ). Hence setting high and low bounds on the ocean bottom conductance is equivalent to setting low and high bounds on  $\bar{\mathbf{u}}_H^*$ . These two limits are shown in Figure 10. We see that the differences in  $\bar{\mathbf{u}}_H^*$  for the low (Figure 10a)

and high (Figure 10b) conductance cases appear to be greatest in shallow areas such as the Bering and Iceland Seas and the Pacific-Indian Throughway (north of Australia). This is due to an increase in the importance of the ocean bottom conductance relative to the total ocean and ocean bottom conductance. The maximum magnitudes of  $\bar{\mathbf{u}}_H^*$  are several tens of centimeters per second.

The horizontal electric field  $\mathbf{E}_H$  shown in Figure 11 is merely  $\bar{\mathbf{u}}_H^*$  weighted by  $F_z$  (see (13)). Hence the shallow-water effects discussed for  $\bar{\mathbf{u}}_H^*$  also apply to  $\mathbf{E}_H$ . The magnitudes of  $\mathbf{E}_H$  reach about  $10 \mu\text{V m}^{-1}$  and are relatively weak in the equatorial regions due to the decrease in  $F_z$ . The vertical component  $E_z$  depends on depth (see (16)). We have plotted  $E_z$  at depths of 100, and 1000 m in Figure 12. The magnitudes of the vertical component tend to be a little higher than those of the horizontal components. Note that  $E_z$  is highest in the equatorial regions and weaker toward the poles because of the latitudinal dependence of  $\mathbf{F}_H$ . Also, current reversals with depth along the equator give reversed  $E_z$  values which have large amplitudes due to the relatively great strength of  $\mathbf{F}_H$  in these regions.

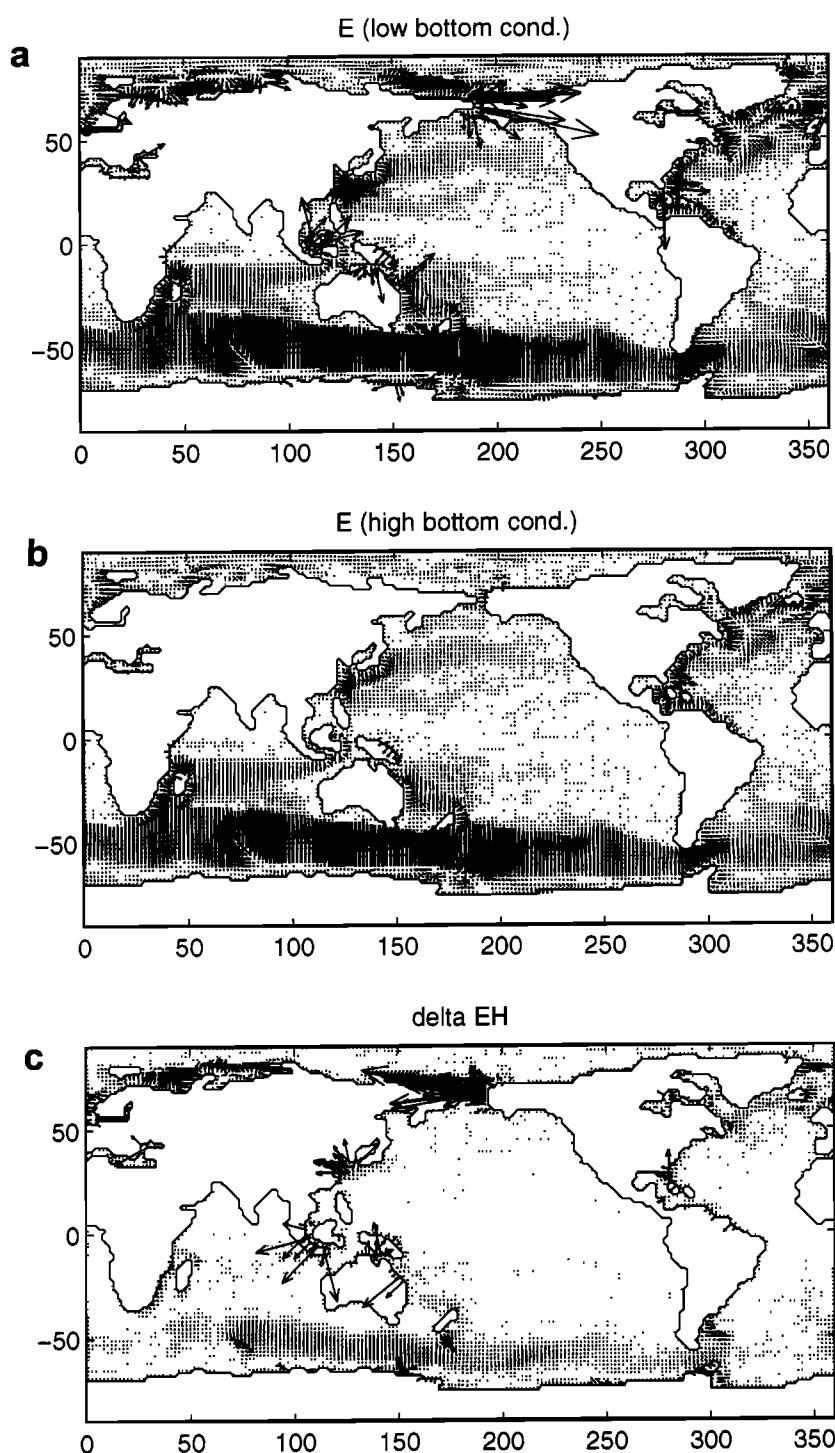


**Figure 11.** Horizontal component of the ocean-induced electric field  $\mathbf{E}_H$  is shown for (a) low, and (b) high, limiting cases of ocean bottom conductance. (c) The difference (i.e. Figure 11b minus Figure 11a) is shown. Scale is  $5^\circ = 10^{-6} \text{ V m}^{-1}$ .

The ocean-induced electric current densities  $\mathbf{J} \approx \mathbf{J}_H$  are calculated at two depths using (14) and are shown in Figures 13 and 14. In areas where  $\mathbf{J}$  is strong, the high- and low-conductivity cases agree quite well over most of the globe. This could be expected from (14) since in areas where  $\mathbf{u}_H$  is much greater than  $\mathbf{u}_H^*$ ,  $\mathbf{J}_H$  depends little on  $\mathbf{u}_H^*$  or the assumptions concerning the ocean bot-

tom conductance. The magnitudes reach about  $6 \times 10^{-5} \text{ A m}^{-2}$ .

The ocean-induced magnetic fields  $\mathbf{b} \approx \mathbf{b}_H$  are shown in Figures 15 and 16 for two depths. The magnitudes of  $\mathbf{b}_H$  tend to increase with depth since they depend on the integral of electric currents in the layer between the depth and the sea surface. The different scales used for

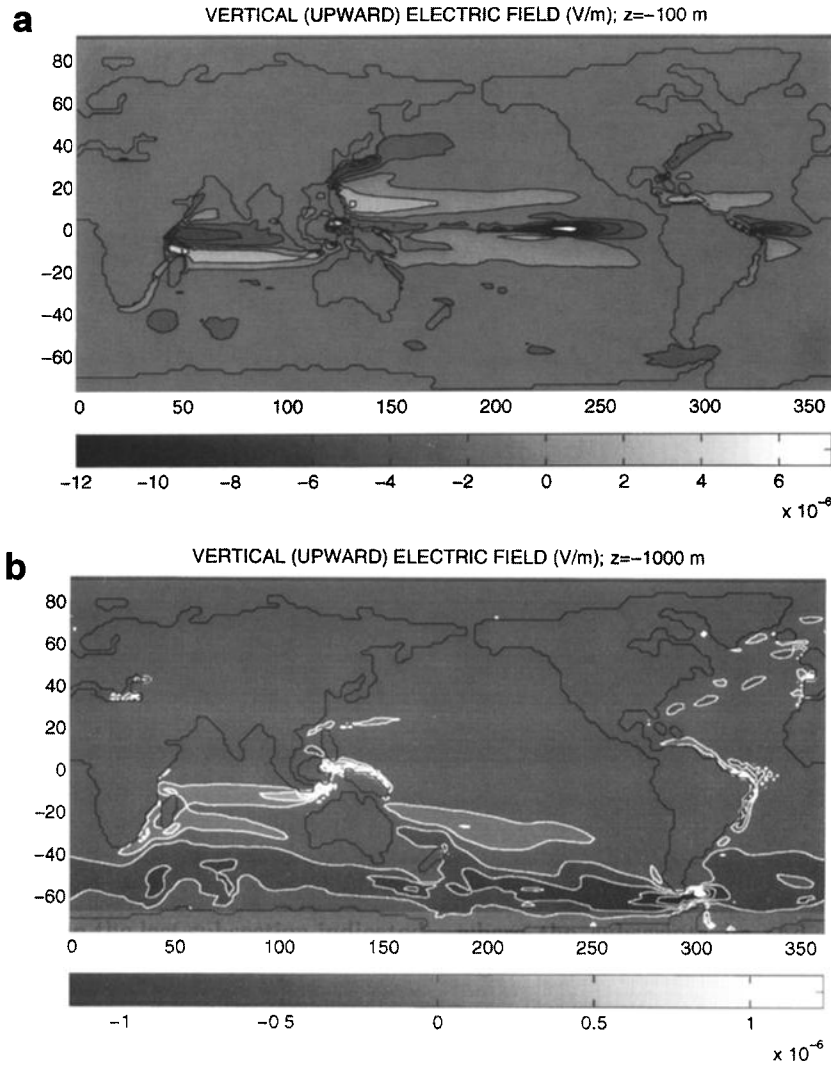


**Figure 12.** Vertical component of the ocean-induced electric field  $E_z$  at (a) 100 m and (b) 1000 m. Units are volts per meter but note that scale on bar varies.

plotting should be noted. The magnitudes reach values of about a couple of nanoteslas (at 20 m), about 10 nT (at 100 m), and a few tens of nanoteslas in the deeper ocean. As can be seen, the two cases produce magnetic fields which are essentially identical at the scales plotted.

It might seem that the uncertainties in the magnetic estimates should increase with depth since the calculation involves integrating over electric currents (together with uncertainties) in the layer 0 to  $z$ . However, we must also consider the following competing effect. In deeper water the bottom conductance becomes a smaller fraction of the total conductance, and hence the decrease in the relative uncertainties in the column conductance leads to a decrease in the uncertainty of the magnetic field. This point is further discussed in the next subsection.

#### 4.4. Fractional Uncertainties

The results presented in the last subsection indicated that the solutions for the dominant ocean-induced elec-

tric currents and magnetic fields were largely insensitive to bottom conductance. It could not be determined from the figures, however, that a similar result applied for regions where the fields were weak. Here we address this by calculating the fractional uncertainties in the EM field estimates. Specifically, using (10) and (13)–(15), the fractional uncertainties are calculated as follows:

$$\frac{|\delta \bar{\mathbf{u}}_H^*|}{|\bar{\mathbf{u}}_{Hlc}^*|} = \frac{\delta \Sigma}{\Sigma_{hc}}, \quad (17)$$

$$\frac{|\delta \mathbf{E}_H|}{|\mathbf{E}_{Hlc}|} = \frac{\delta \Sigma}{\Sigma_{hc}}, \quad (18)$$

$$\frac{|\delta \mathbf{J}_H|}{|\mathbf{J}_{Hhc}|} = \frac{\delta \Sigma}{\Sigma_{hc}} \frac{|\bar{\mathbf{u}}_{Hhc}^*|}{|\mathbf{u}_H - \bar{\mathbf{u}}_{Hlc}^*|}, \quad (19)$$

$$\frac{|\delta \mathbf{b}_H|}{|\mathbf{b}_{Hhc}|} = \frac{\delta \Sigma}{\Sigma_{hc}} \frac{\int_z^0 \sigma dz}{\int_z^0 \frac{\sigma(\mathbf{u}_H - \bar{\mathbf{u}}_{Hlc}^*)}{|\bar{\mathbf{u}}_{Hhc}^*|} dz}, \quad (20)$$

where the subscripts  $hc$  and  $lc$  refer to the cases of high and low bottom conductance, respectively,  $\delta \bar{\mathbf{u}}_H^* =$

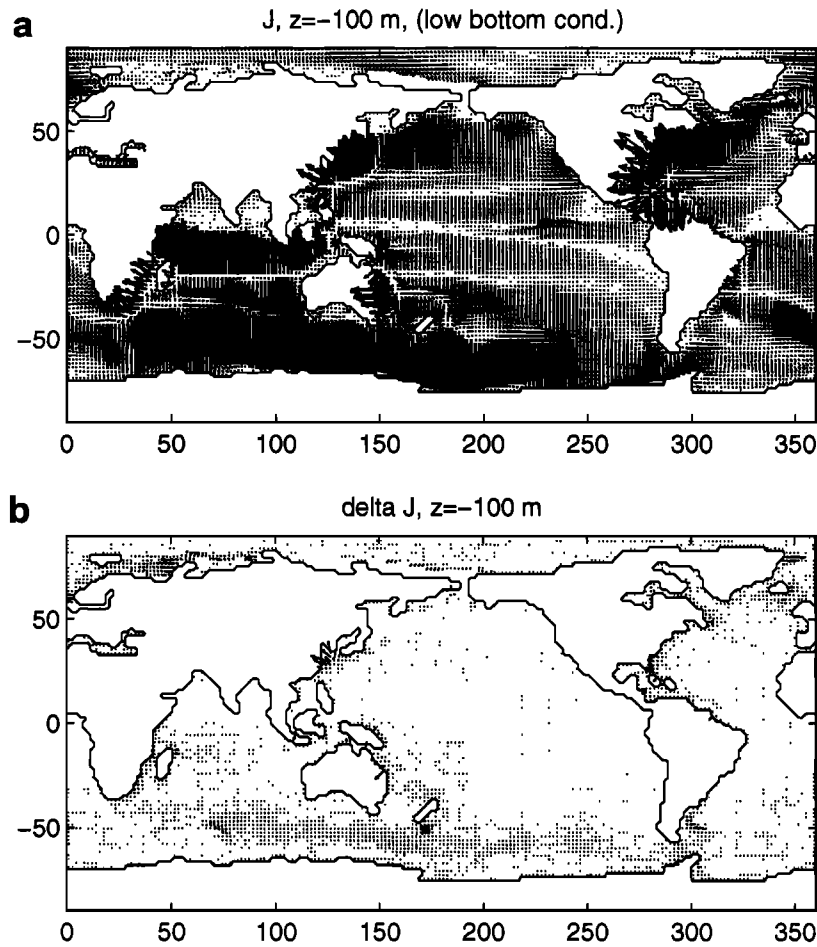


**Figure 13.** (a) Ocean-induced electric current density  $\mathbf{J} \approx \mathbf{J}_H$  at 100-m depth is shown for the limiting case of low bottom conductance. (b) The difference (high minus low) between the two cases of high and low bottom conductance is shown. Scale is  $5^\circ = 10^{-5} \text{ A m}^{-2}$ .

$\bar{\mathbf{u}}_{Hhc}^* - \bar{\mathbf{u}}_{Hlc}^*$  (and similar for  $\delta \mathbf{E}_H$ ,  $\delta \mathbf{J}_H$ ,  $\delta \mathbf{b}_H$ ), and  $\delta \Sigma / \Sigma_{hc}$  is simply the fractional uncertainty in the total (ocean + sediment) conductance. Note that in the specific cases we plotted where the low bottom conductance is taken to be zero,  $\delta \Sigma / \Sigma_{hc}$  is equivalent to the factor  $\lambda / (1 + \lambda)$  given by Sanford [1971].

The fractional uncertainty in  $\bar{\mathbf{u}}_H^*$  (and similarly in  $\mathbf{E}_H$ ) is depth independent and simply varies with the fractional uncertainty in the conductance. As can be seen in Figure 17, this largely follows the ocean layer conductance (shown in Figure 8), which makes sense since in deeper or warmer waters where the ocean conductance is greatest, the relative importance of the sediment conductance in the total column conductance is reduced.

In the denominators of (17) and (18) we used magnitudes for  $\bar{\mathbf{u}}_H^*$  and  $\mathbf{E}_H$  assuming the low bottom conductivity case. Since  $\bar{\mathbf{u}}_H^*$  and  $\mathbf{E}_H$  will generally be reduced by including the conductive sediment, these equations and Figure 17 can be interpreted as describing a bound on the amount  $\bar{\mathbf{u}}_H^*$  and  $\mathbf{E}_H$  would be overestimated while calculating  $\bar{\mathbf{u}}_H^*$  and  $\mathbf{E}_H$ , assuming zero

bottom conductance. The electric currents and magnetic fields, however, will usually increase with sediment conductance. Hence (19) and (20) use the high-conductance magnitudes ( $|\mathbf{J}_{Hhc}|$ ,  $|\mathbf{b}_{Hhc}|$ ) in the denominator and will generally describe maximum overestimates in  $|\mathbf{J}_H|$  and  $|\mathbf{b}_H|$  when calculated assuming the high-conductance model. If no interpretation of the sign of the uncertainty error were sought, the EM quantities could be calculated for a bottom-conductance case midway between the high and low models. A reformulation of (17)–(20) using the new midway magnitudes in the denominators would then give smaller relative uncertainties.

As seen in (19) and (20), the fractional uncertainties in  $|\mathbf{J}_H|$  and  $|\mathbf{b}_H|$  depend again on the fractional uncertainty in the conductance but also depend on the relative velocities. At a point where the velocity is much greater than  $\bar{\mathbf{u}}_H^*$ , the uncertainty in  $\mathbf{J}_H$  will be small. From Figure 18a we see that near the sea surface (where velocities are often greatest), the uncertainty in  $\mathbf{J}_H$  is down to a couple of percent or less. In contrast, at depth (see Figure 18b) where the velocities are not usually

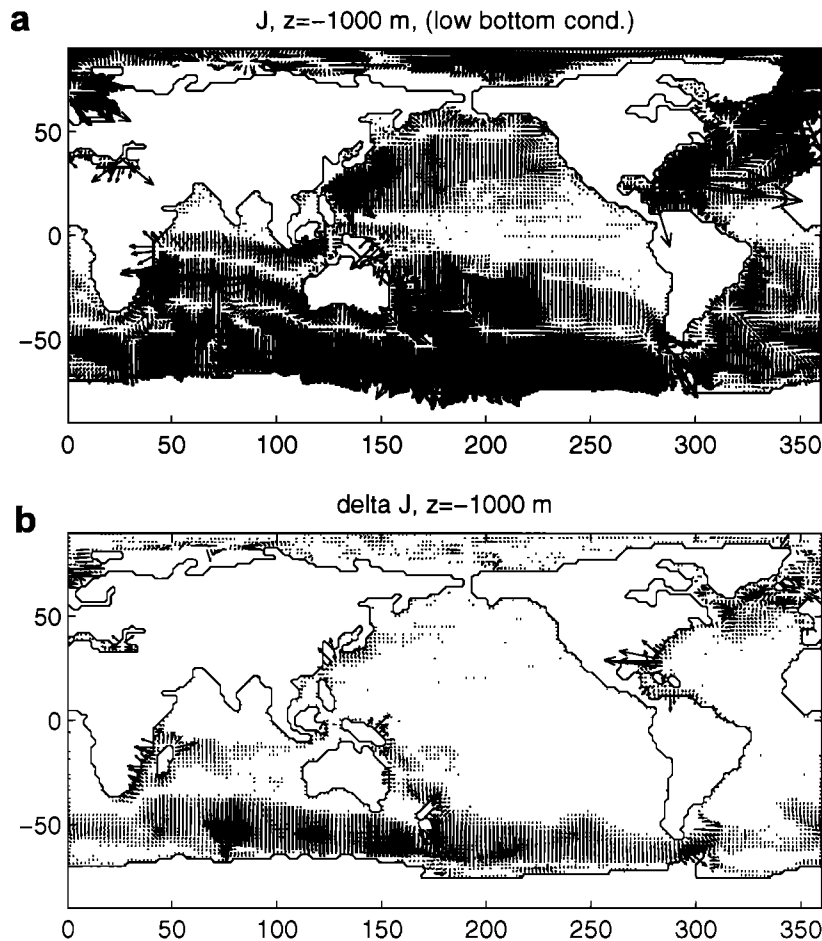


**Figure 14.** (a) Ocean-induced electric current density  $\mathbf{J} \approx \mathbf{J}_H$  at 1000-m depth is shown for the limiting case of low bottom conductance. (b) The difference (high minus low) between the two cases of high and low bottom conductance is shown. Scale is  $5^\circ = 10^{-5} \text{ A m}^{-2}$ .

much greater than  $\bar{\mathbf{u}}_H^*$ , the relative errors are greater than 20% over most of the ocean.

From (20), the fractional uncertainty in  $\mathbf{b}_H$  will be low when the volume transport in the layer between the depth  $z$  and the sea surface is much greater than the thickness of the layer multiplied by  $\bar{\mathbf{u}}_H^*$ . Hence, since much of the ocean circulation is surface intensified, we should expect the fractional uncertainties in  $\mathbf{b}_H$  to be small even at great depths. Indeed, Figure 19 shows that even at 1000-m depth, the uncertainties in  $\mathbf{b}_H$  are often only a couple percent.

## 5. Nonlocal Electric Currents

We have assumed in this work that the ocean-generated electric currents close predominantly in planes containing the vertical. In a typical case of surface-intensified flow in the northern magnetic hemisphere, electric currents would move to the left of the flow at the surface and return below in the deeper ocean and sediment layer to close a loop. In reality, the ocean-generated electric fields will also create electric currents closing in horizontal planes. If these nonlocal currents were included,

the results obtained would be different than those we obtained above: by how much? The goal of this section is simply to indicate that corrections for the nonlocal currents are not worthwhile until corrections for the sediment conductance are made.

The nonlocal electric currents are important not only because they tend to reduce locally generated electric fields (and complicate the use of electric field observations to measure ocean flow) but also because these currents are responsible for magnetic signals which occur outside and above the ocean and which, if strong enough, might be observed at satellite altitudes to remotely sense characteristics of ocean flow [Tyler, 1995]. So far, however, the nonlocal electric currents have not been sufficiently studied. Two of us (R.H.T and J.M.O) together with T. B. Sanford have work underway to estimate these effects. In this paper, we have restricted the focus on getting a basic picture of the EM fields generated by global ocean circulation. Hence, regarding the nonlocal currents, we need merely show next that the uncertainties due to the nonlocal effects are usually less than the uncertainties due to the sediment conductance.

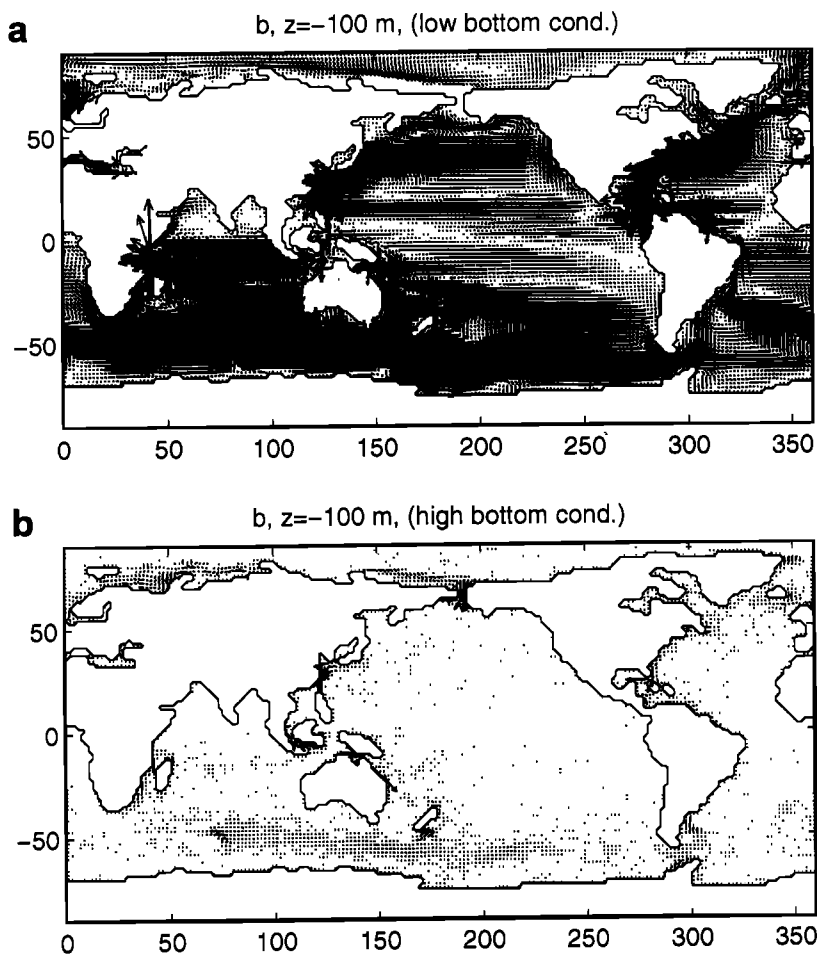


**Figure 15.** (a) Ocean-induced magnetic field  $\mathbf{b} \approx \mathbf{b}_H$  at 100-m depth is shown for the limiting case of low bottom conductance. (b) The difference (high minus low) between the two cases of high and low bottom conductance is shown. Scale is  $5^\circ = 1 \text{ nT}$ .

In the steady state, the electric field can be written as the gradient of a scalar  $-\phi$ , and the electric currents are nondivergent ( $\nabla \cdot \mathbf{J} = 0$ ). Using approximations consistent with those described earlier, the divergence of the depth integral of Ohm's law gives a two-dimensional electropotential equation:

$$\nabla \cdot [\Sigma (\nabla_H \phi - F_z \hat{\mathbf{u}}_H \times \hat{\mathbf{z}})] = 0, \quad (21)$$

where  $\Sigma$  is the conductance and  $F_z$  is the vertical (radial) component of the Earth's main magnetic field.

Equation (5) was solved within the OPYC code to produce the electropotential shown in Figure 20 (see the Appendix for a description of the solution technique). To maximize the potential effect of the nonlocal electric currents, we assumed zero conductance for the ocean bottom and continents. Outside of limited regions such as the Bering Strait, the results are in basic agreement with the electropotential calculated by *Stephenson and Bryan* [1992, Figure 4] for the simplified case of uniform ocean conductivity.

The "true" electric field  $-\nabla \phi$  will generally be smaller than the corresponding electric field  $\mathbf{E}_H$  (low bottom

conductance case) we calculated above while neglecting the nonlocal currents. (Note, however, that in regions where the ocean currents are extremely small, the fractional errors in neglecting nonlocal currents become large because the EM field magnitudes are very small.) The differences in the two electric field estimates ( $-\nabla \phi$  and  $\mathbf{E}_{Hlc}$ ) were seen to be smaller than the rather large differences between the estimates for the two bottom conductance assumptions. Hence it appeared that including the nonlocal currents would not improve the EM estimates unless the bottom conductance was first realistically modeled.

Perhaps most importantly, the finding that over much of the ocean the dominant electric currents and magnetic fields were not sensitive to bottom conductance can be extended to include an insensitivity to the nonlocal effects. That is, physically, it could be stated that the dominant electric currents induced by ocean circulation close in vertical-plane loops within the water. Secondary electric currents may flow in horizontal planes or vertical planes extending into the ocean floor. In Figure 21 we have plotted a couple of examples in support of the statements above. Figures 21a and 21b should be

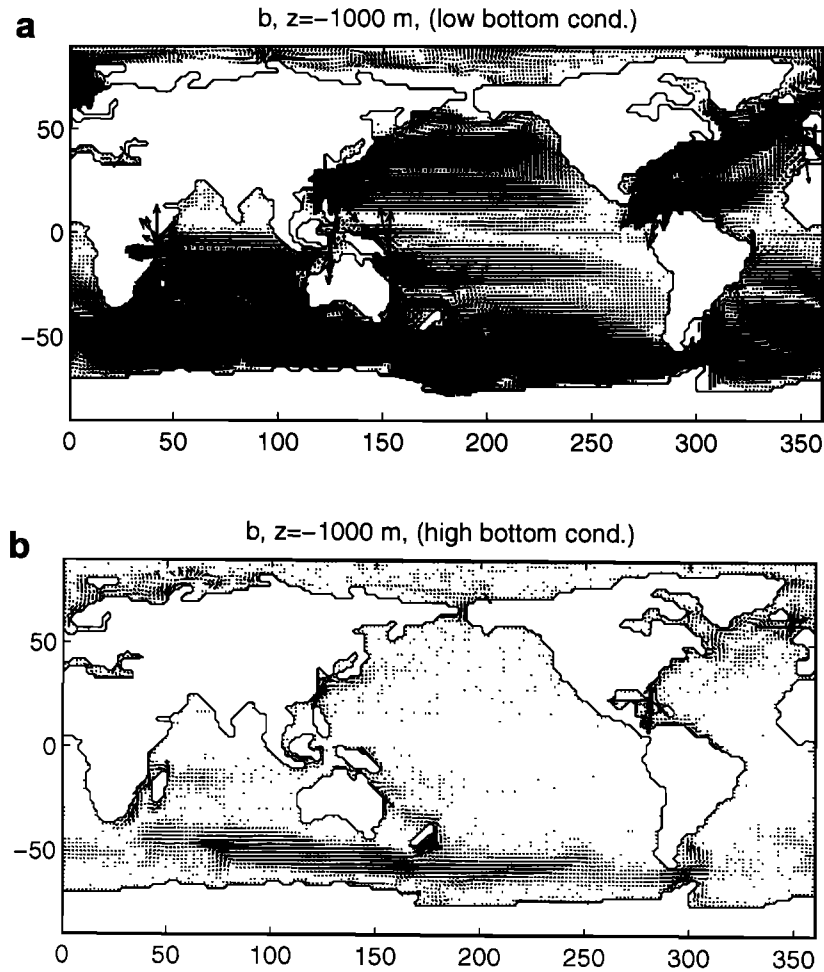


**Figure 16.** (a) Ocean-induced magnetic field  $b \approx b_H$  at 1000-m depth is shown for the limiting case of low bottom conductance. (b) The difference (high minus low) between the two cases of high and low bottom conductance is shown. Scale is  $2^\circ = 1$  nT.

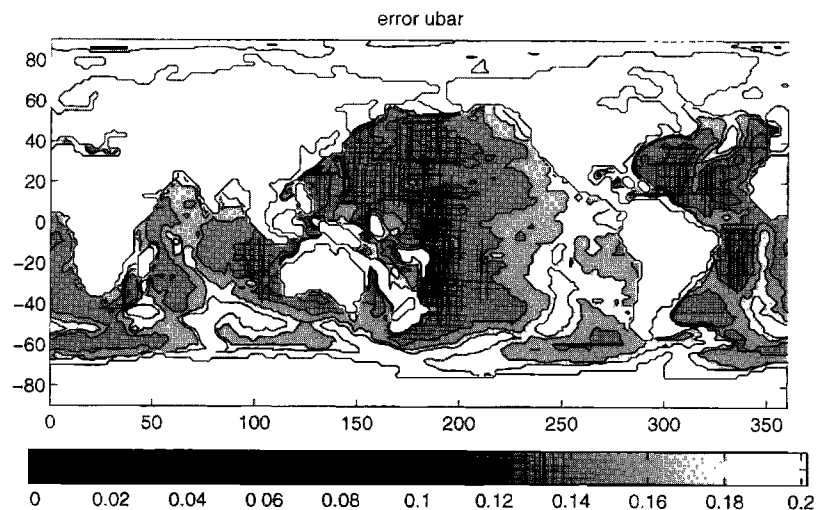


**Figure 17.** Shown are the fractional uncertainties in  $\bar{u}_H^*$  due to the differences between the two ocean bottom-conductance assumptions. Over much of the deeper ocean, the uncertainty ranges from about 10 to 20%. This figure describes equally the fractional uncertainties in  $E_H$ .



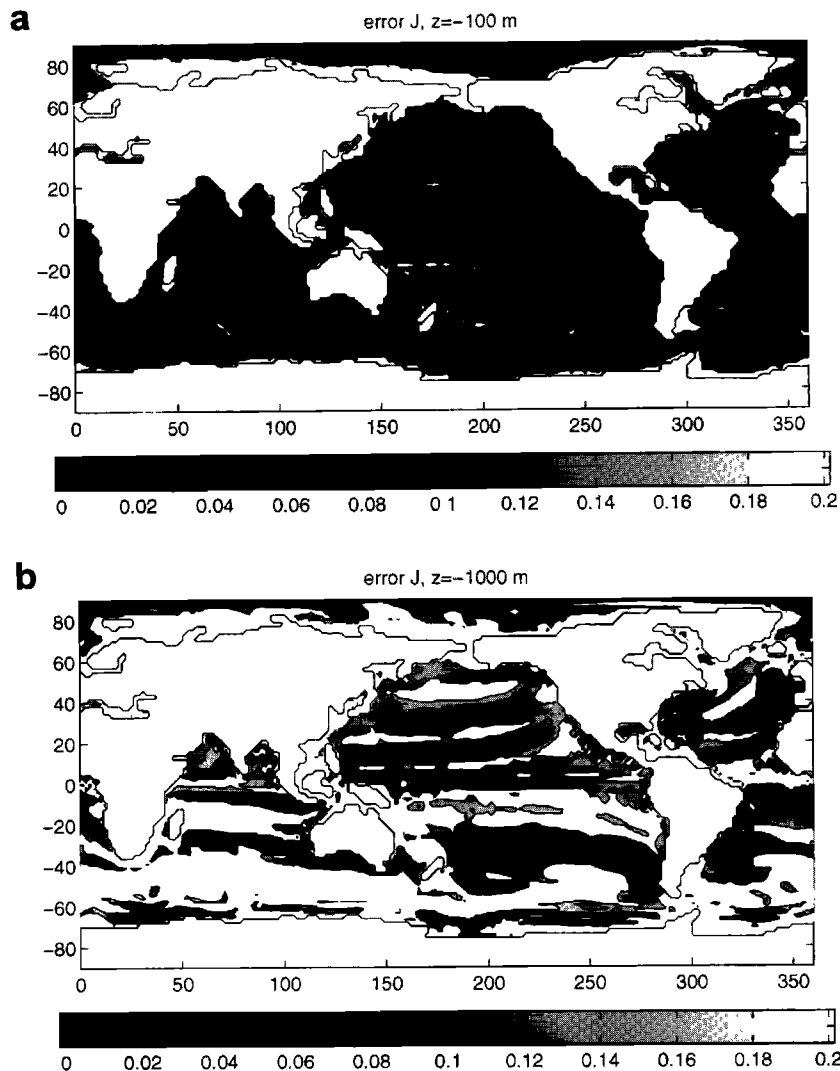


**Figure 18.** Shown are the fractional uncertainties in  $J_H$  due to the differences between the two ocean bottom-conductance assumptions. While the uncertainties are only a couple of percent (a) at 100 m depth, (b) at 1000-m depth, about half the ocean has an uncertainty greater than 20%.

compared with Figures 13b and 14b, respectively, and are plotted on the same scales. We see clearly that the uncertainties due to the nonlocal effects are generally even less than the uncertainties due to the bottom conductance. Uncertainties due to either effect only appear to become an issue in deeper water.

## 6. Discussion and Summary

In general, to solve for the electromagnetic fields generated by the motion of the electrically conductive ocean through the Earth's main magnetic field, we would have to solve a global problem; the EM field at one point would depend on the ocean state and electrodynamics at all other points. To solve for the EM fields generated by steady ocean circulation would require then a three-dimensional integration over a globe resolving the oceans and the conductive ocean bottom and continents.

Here we have obtained global EM solution more simply by making certain approximations and considering two limiting cases. The approximations are largely related to the aspect ratio of the ocean flow and conductivity fields and allow us to obtain solutions from at most a 1-D vertical integration at each point rather than from a 3-D integration. The conductance distribution below the ocean is a relevant quantity but is quite inhomogeneous and is difficult to estimate. We address this by finding EM solutions for two cases using limiting assumptions for the ocean bottom conductance. In one case we assume the region below the ocean is an electrical insulator, and in the second we assume a sediment conductance of  $3000 \text{ S m}^{-1}$ , which we regard as a maximum large-scale local average.

The study illustrates that many aspects of the ocean-generated EM fields are not sensitive to the ocean bottom-conductance distribution. This has practical significance since, for example, it is easier to use EM

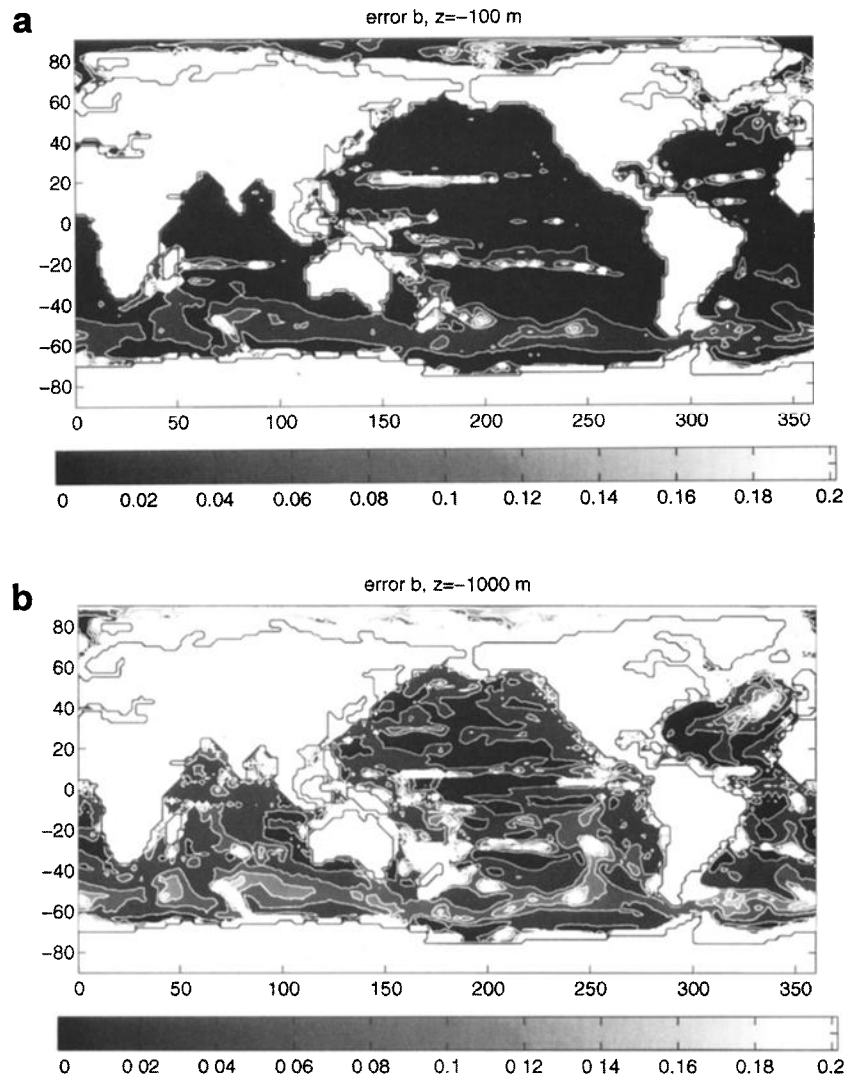


**Figure 19.** Shown are the fractional uncertainties in  $b_H$  due to the differences between the two ocean bottom-conductance assumptions. The uncertainties are rather low both at depths of (a) 100 m and (b) 1000 m.

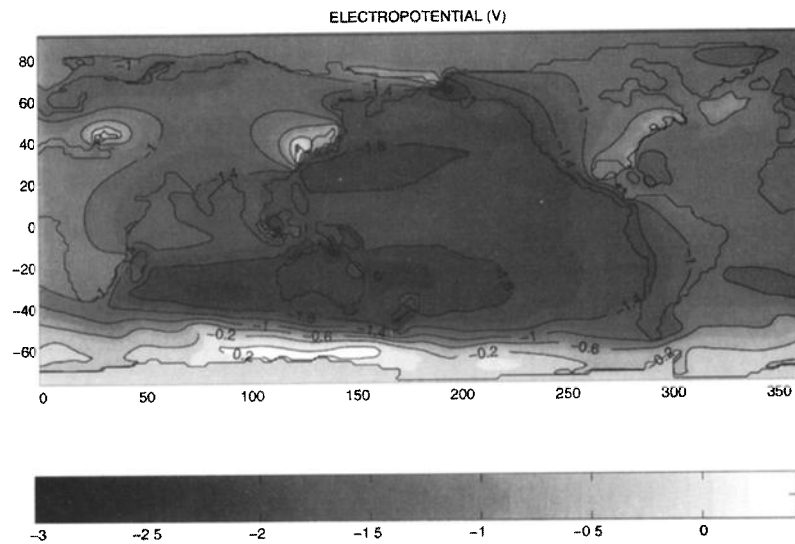


**Figure 20.** Electropotential due to steady ocean circulation (volts).

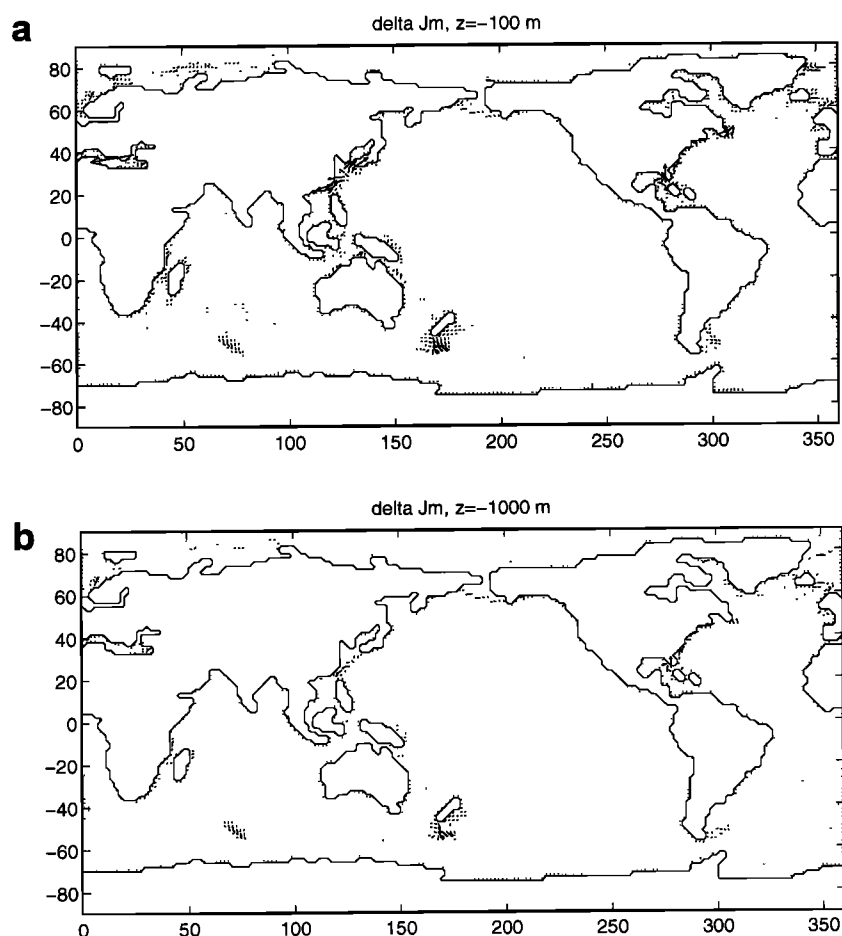


**Figure 21.** Shown is an example of the electric currents (at depths of (a) 100 m and (b) 1000 m) calculated including nonlocal effects minus the electric currents calculated assuming the simplified model (for low bottom-conductance case). Figures 21a and 21b should be compared to Figures 13b and 14b to see that uncertainties in the nonlocal effects are at least as small as the effects of uncertainties due to unknown sediment conductance.

measurements to determine ocean flow where an accurate description of the ocean bottom conductance is not required. Conversely, areas where the ocean-generated EM fields are sensitive to ocean bottom conductance may offer prime opportunities for using the ocean EM fields to study the geological composition below the ocean.

In the calculations and for the framework of the following discussion, we assume that the ocean state is known and we wish to calculate the ocean-generated EM fields. The uncertainty in the sediment conductances then creates an uncertainty in the estimated EM fields. (In a practical application, perhaps the EM fields are measured and the uncertainties in bottom conductance then translate as uncertainties in the estimated ocean velocities.)

The ocean-generated horizontal electric currents reach magnitudes of about  $10 \mu\text{V m}^{-1}$  and tend to be greatest in areas of large volume transport or strong flow in shallow water. The effect of sediment conductance is generally to reduce the electric fields. We find that

the fractional uncertainties in the horizontal electric field depend directly on the fractional uncertainty in the ocean bottom conductance (described by (17) and Figure 17). In our examples, the horizontal electric field typically has an uncertainty of 15% or more. Hence precise determination of ocean flow from horizontal electric field measurements requires consideration of the realistic ocean bottom conductance for the site. This is known and is conventionally employed. Of greater difficulty, however, will be areas where there are strong lateral variations in the fractional conductance uncertainties. As an example, *Spain and Sanford [1987]* attribute the ability to use voltage differences across a submerged cable spanning a section of the Florida Current to the fact that the conductance was rather uniform. Conversely, at sections with nonuniform conductance, lateral shifts in the Florida Current might be misinterpreted as changes in transport. Interestingly, *Spain and Sanford* also point out that increased bottom conductance actually helps the endeavor since though the magnitude of the electric field (potential difference)

is reduced, the sensitivity of the potential difference on the distribution of transport and electrical conductance becomes less. That is, with higher bottom conductance, less needs to be known about the nonuniformities in flow and conductivity to determine the total transport from voltage measurements.

The vertical component of the electric field depends on depth and was seen to have a magnitude comparable to that of the horizontal components. The geographic distribution, however, is quite different: while the horizontal components are greater toward the poles, the vertical component is greatest near the equator where the horizontal component of the Earth's main magnetic field is maximum. We have not analyzed the dependence of the vertical electric field on the ocean bottom conductance. While the types of calculations we have done would indicate that this component is not sensitive to bottom conductance, a more appropriate analyses should probably consider lateral inhomogeneities in flow and conductivity.

Scaling arguments determined that the vertical electric currents are much smaller than the horizontal components. The horizontal components have magnitudes of about  $60 \mu\text{A m}^{-2}$ , and are strongest in regions where, roughly, the velocities are faster than their depth averages. The fractional uncertainties in the electric currents depend not only on the fractional uncertainties in bottom conductance but also on the velocity relative to the depth-averaged velocity (or, more accurately,  $\bar{u}_H^*$ ). Hence areas where the electric currents are strong are coincident with areas where the fractional uncertainty is small. Reflecting the fact that much of the ocean flow is surface intensified, we saw that uncertainties in the electric currents at a depth of 100 m were only a couple of percent compared to at a kilometer depth where the uncertainties were greater than 20% over about half the global ocean.

The dominant magnetic fields are directed horizontally and are confined to the oceans. The magnitudes are several nanoteslas near the sea surface but reach over 100 nT at depth. The magnetic field at depth  $-z$  depends essentially on the depth integral of electric currents between  $z$  and the sea surface ( $z = 0$ ). Hence, as might be expected, even though the uncertainties in the electric currents might become large with depth, the uncertainties in the magnetic field remain small. Even at a kilometer depth, most of the ocean had magnetic field uncertainties of less than 5%.

Where the results presented here overlap with observations and modeling studies, there is general agreement. The typical magnitudes of the EM fields described above match observed values. In particular, the voltage difference that would be obtained from integrating our electric field across the Florida Current is about 1.0 V, slightly under the observed values of about 1.2 V [Spain and Sanford, 1987]. The electric current and magnetic fields we find are also in general agreement with observations but may be half as large

as fields indicated from energetic transient ocean features. (Maximum magnetic fields inferred from seafloor EM measurements of a strong eddy reached about 250 nT [Lilley et al., 1993].) Also, the root-mean-square magnitude of the electric field in the North Atlantic from the high-resolution Flosadóttir et al. [1997] model study is slightly higher than what we calculate. This should be expected since the EM fields calculated from the steady large-scale circulation will be weaker than EM fields from realistic currents including small-scale and transient features. Although the solution for the ocean electropotential was included here only to validate the simpler approach, we can point out that the electropotential (Figure 20) agrees quite well with that calculated by Stephenson and Bryan [1992] even though the ocean state and conductivity fields used were different. However, in certain limited regions, such as the Bering Strait, the results are quite different, likely reflecting the higher resolution used for this study.

We assumed that the electric currents close in planes containing the vertical axis. The fact that the electric currents and magnetic fields were insensitive to bottom conductance simply means that the electric currents close predominantly within the ocean and little passes through the sediments. A realistic case, however, would also allow electric currents to close in horizontal planes. This could be important, for example, because locally generated electric fields in areas of strong flow would tend to be reduced by these horizontal currents. Similarly, in areas of sluggish flow, the electric fields might be due to electric charge densities established entirely by flow elsewhere.

Without trying to downplay the general importance of these horizontal-plane nonlocal electric currents, we show that their effect on the dominant fields measured within the water is usually less than that of the sediment conductance. Our finding is simply that including nonlocal electric currents does not help until the sediment conductance is first modeled realistically. In some cases, valuable oceanographic information may be obtained from EM observations without modeling either of these effects. In other cases, the sediments are being modeled realistically and the question of how these studies might be improved by including nonlocal effects is important. For the results we have presented could be turned around to say, "including sophisticated models of the sediment conductivity is not worthwhile unless the nonlocal effects are also included".

While the nonlocal electric currents appear to play a secondary role in the dominant ocean-generated EM field within the ocean, which we have addressed in this paper, the nonlocal electric currents have an extremely important role in the generation of EM fields outside of the ocean. Our results regarding the neglect of the nonlocal effects should not be extended beyond the application here.

We wish to emphasize that we have not run a global numerical model to obtain the EM fields we have plot-

ted. (We did run a global numerical model but just to produce results to validate our simple calculations. Only Figures 20 and 21 involve these global numerical results.) The EM fields we have calculated involve at most vertical integrations. This is an important point. If EM fields could only be associated with ocean flow once a global model was run involving knowledge of the global ocean state, then the practical utility of using EM measurements in oceanography would be greatly reduced.

## Appendix: Electropotential Solution Technique

The method to solve (5) uses a mixture between a direct and an iterative solution method. Each step within the iteration consists of two parts. The first one solves the  $x$  direction directly based on a tridiagonal linear equation. This means that the  $x$  derivatives appear as matrix coefficients, while the derivatives in  $y$  direction are treated as in an overrelaxation technique. This means that the center point appears in the matrix while the neighboring points appear at the right-hand side as some forcing. This linear equation system in the  $x$  direction is written down for all even  $y$  indices and solved in parallel. Then the linear equations for all odd  $y$  indices are solved. The second part consists of the same scheme; however, now the  $y$  direction is treated directly and the  $x$  direction is treated iteratively. These two steps are repeated until convergence as deduced from the error in (5) is achieved. The method is a compromise between a full linear equation system, which has the disadvantage of being huge, and an iterative method, which has the advantage of being simple, but is more expensive due to a potential slow convergence. In fact, (5) is poorly conditioned for iterative methods because the conductance varies over orders between the oceans and continents. However, if the system is formulated as a linear equation system, only round-off problems matter. In the chosen method we have gained the advantage that the direct solution method, which is based on tridiagonal matrices, couples each grid point during each iteration and thus allows a quick error reduction in the equation. The only disadvantage compared with a fully direct solution method is that we still need to iterate.

For the horizontal boundary condition, a predefined value for the south pole is assumed, e.g., zero. The value across the north pole is constructed as for temperature or salinity in the ocean model. After rotating all individual cross-polar gradients of the potential onto a common tangential plane and calculating a mean gradient across the pole, all individual points in the  $x$  direction across the pole obtain a potential which is estimated by extrapolation from the polar mean value and the back-rotated gradients of the potential. During the iteration, values around the pole then smoothly adjust

without requiring an additional boundary condition as some polar value or some gradient.

**Acknowledgments.** This work has greatly benefited from suggestions by two anonymous reviewers. R. H. T. would like to thank Tom Sanford and Agústa Flosadóttir for helpful discussions. L. A. M. gratefully acknowledges the support of the Canadian Natural Sciences and Engineering Research Council for this work. J. M. O. is grateful to the Ministry of Education and Research, BMBF, Germany.

## References

- Apel, J. R., *Principles of Ocean Physics*, 634 pp., Academic, San Diego, Calif., 1987.
- Bindoff, N. L., J. H. Filloux, P. J. Mulhearn, and F. E. M. Lilley, Vertical electric field fluctuations at the floor of the Tasman abyssal plain, *Deep Sea Res., Part A*, **33**, 587–600, 1986.
- Chave, A. D., On the theory of electromagnetic induction in the Earth by ocean currents, *J. Geophys. Res.*, **88**, 3531–3542, 1983.
- Chave, A. D., and D. S. Luther, Low-frequency, motionally induced electromagnetic fields in the ocean, *J. Geophys. Res.*, **95**, 7185–7200, 1990.
- Chave, A. D., S. C. Constable, and R. N. Edwards, *Electrical Exploration Methods for the Seafloor*, vol. 2, chap. 12, pp. 931–965, Soc. of Explor. Geophys., Tulsa, Okla., 1988.
- Chave, A. D., A. H. Flosadóttir, and C. S. Cox, Some comments on seabed propagation of ULF/ELF electromagnetic fields, *Radio Sci.*, **25**, 825–836, 1990.
- Filloux, J. H., in *Geomagnetism*, vol. 1, chap. 3, Instrumentation and experimentation methods for oceanic studies, pp. 143–248, Academic, San Diego, Calif., 1987.
- Flosadóttir, A. H., J. C. Larsen, and J. T. Smith, Motional induction in North Atlantic circulation models, *J. Geophys. Res.*, in press, 1997.
- Larsen, J. C., An introduction to electromagnetic induction in the ocean, *Phys. Earth Planet. Inter.*, **7**, 389–398, 1973.
- Larsen, J. C., Transport and heat flux of the Florida Current at 27° N derived from cross-stream voltages and profiling data: Theory and observations, *Phil. Trans. R. Soc. London Ser. A*, **333**, 169–236, 1992.
- Larsen, J. C., and T. B. Sanford, Florida Current volume transports from voltage measurements, *Science*, **227**, 302–303, 1985.
- Lilley, F. E. M., J. H. Filloux, N. L. Bindoff, I. J. Ferguson, and P. J. Mulhearn, Barotropic flow of a warm-core ring from seafloor electric measurements, *J. Geophys. Res.*, **91**, 12,979–12,984, 1986.
- Lilley, F. E. M., J. H. Filloux, P. J. Mulhearn, and I. J. Ferguson, Magnetic signals from an ocean eddy, *J. Geomag. Geoelectr.*, **45**, 403–422, 1993.
- Macdonald, A. M., Property fluxes at 30°S and their implications for the Pacific-Indian throughflows and the global heat budget, *J. Geophys. Res.*, **98**, 6851–6868, 1993.
- Oberhuber, J. M., The opyc ocean general circulation model, *Tech. Rep.* 7, 130 pp., Dtsh. Klimarechenzentrum GmbH, Hamburg, Germany, 1993a.
- Oberhuber, J. M., Simulation of the Atlantic circulation with a coupled sea ice - mixed layer - isopycnal general circulation model, I, Model description, *J. Phys. Oceanogr.*, **22**, 808–828, 1993b.
- Sanford, T. B., Motionally induced electric fields in the sea, *J. Geophys. Res.*, **76**, 3476–3493, 1971.
- Sanford, T. B., Temperature transport and motional induction in the Florida current, *J. Mar. Res.*, **40**, 621–639, 1982.

- Schmitt, R. W., The ocean component of the global water cycle, *U. S. Nat. Rep. Int. Union Geod. Geophys. 1991-1994*, *Rev. Geophys.*, **33**, 1395-1409, 1995.
- Schmitz, W. J. J., On the interbasin-scale thermohaline circulation, *Rev. Geophys.*, **33**, 151-173, 1995.
- Spain, P., and T. B. Sanford, Accurately monitoring the Florida current with motionally induced voltages, *J. Mar. Res.*, **45**, 843-870, 1987.
- Stephenson, D., and K. Bryan, Large-scale electric and magnetic fields generated by the oceans, *J. Geophys. Res.*, **97**, 15,467-15,480, 1992.
- Tyler, R. H., Electromagnetic fields generated by ocean currents and the potential for using geomagnetic data in ocean and climate studies, Ph.D. thesis, McGill Univ., Montréal, Quebec, Canada, 1995.
- Tyler, R. H., and L. A. Mysak, Electrodynamics in a rotating frame of reference with application to global ocean circulation, *Can. J. Phys.*, **73**, 393-402, 1995a.
- Tyler, R. H., and L. A. Mysak, Motionally-induced electromagnetic fields generated by idealized ocean circulation, *Geophys. Astrophys. Fluid Dyn.*, **80**, 167-204, 1995b.

---

L. Mysak, Centre for Climate and Global Change Research, McGill University, 805 Sherbrooke Street West, Montréal, Québec, Canada H3A2K6. (email: [mysak@zephyr.meteo.mcgill.ca](mailto:mysak@zephyr.meteo.mcgill.ca))

J. Oberhuber, Deutsches Klimarechenzentrum GmbH, Bundesstrasse 55, D-20146 Hamburg, Germany.

R. Tyler, Applied Physics Laboratory, University of Washington, 1013 NE 40th Street, Seattle, WA 98105. (email: [tyler@apl.washington.edu](mailto:tyler@apl.washington.edu))

(Received December 5, 1995; revised September 12, 1996; accepted October 15, 1996.)